Bulletin of Earthquake Engineering (2019) 17:211–235
https://doi.org/10.1007/s10518-018-0445-2

ORIGINAL RESEARCH

Seismic fragility assessment of infilled frames subject to mainshock/aftershock sequences using a double incremental dynamic analysis approach

Fabio Di Trapani[1] · **Marzia Malavisi**[1]

Received: 27 April 2018 / Accepted: 6 August 2018 / Published online: 11 August 2018

Abstract

The paper presents an assessment framework aimed at evaluating seismic fragility and residual capacity of masonry infilled reinforced concrete (RC) frames subject to mainshock/aftershock sequences. A double incremental dynamic analysis (D-IDA) approach is used, based on the combination of a mainshock (MS) signal at different intensities with a set of spectrum-compatible aftershocks (AS) scaled in amplitude with respect to peak ground acceleration. Limit state functions, specifically defined for infilled frames, are used to detect chord-rotation exceeding and shear collapse of RC members during standard and double incremental dynamic analyses. Intact and aftershock fragility curves are obtained for a reference full-scale RC frame specimen, by simulating seismic response with and without infills through a fully fiber section model developed in OpenSees. D-IDA results allow also defining aftershock residual capacity domains and loss diagrams, which are used to compare responses of bare and infilled frames subject to increasing MS intensities. Results show that masonry infills can drastically reduce seismic fragility of RC frame structures during main events and AS, and also limit and economic losses for the mid-low intensity earthquakes. Such beneficial contributions, however, depend on the capacity of RC members to support additional shear demand due frame-infill interaction and avoid sudden failures which conversely occur.

Keywords Incremental dynamic analysis · Fragility curves · Masonry infilled frames · Reinforced concrete · Fiber-section · OpenSees

1 Introduction

Seismic events are generally followed by a number of shakings (aftershocks) due to multiple ruptures of the fault system even at different locations. Cascading shakings have been observed in recent earthquakes L'Aquila (Italy, 2009), Amatrice (Italy, 2016), Tohoku (Japan, 2011), Christchurch (New Zealand, 2010–2011), Chile (2010), Nepal (2015),

✉ Fabio Di Trapani
fabio.ditrapani@polito.it

[1] Dipartimento di Ingegneria Strutturale, Edile e Geotecnica, Politecnico di Torino, Corso Duca degli Abruzzi 24, 10121 Turin, Italy

Kumamoto (Japan, 2016). Buildings may result more or less sensitive to subsequent earthquakes. Damage induced by the main event (mainshock) modifies the overall strength and stiffness and consequently dynamic response to aftershock signals which, on the other hand, may present significantly different frequency content with respect to the first ground motion. Hence, when an aftershock occurs, a different structure, with reduced resistance and lower stiffness, faces a new earthquake, with different intensity and frequency content. The interest in assessing mainshock/aftershock response has grown in the last years, thanks also to the potentiality offered by the recent computer programs in addressing seismic simulations with refined models. A number of researchers have recognized the need for assessing the response of structures subjected to earthquake sequences, highlighting also some deficiencies of technical codes in accounting additional displacement demand from aftershock events. Among these Amadio et al. (2003), and Fragiacomo et al. (2004), analysed SDOF systems and simple steel structures subject to multiple earthquake, evidencing the need for a reduction of the *q*-factor used in design codes to account for the increased ductility demand due to damage accumulation. Similar conclusion were drawn by Di Sarno (2013) after analysing a reinforced concrete sample frame. Hatzigeorgiou and Liolios (2010) and after Hatzivassiliou and Hatzigeorgiou (2015), provided extended analyses of different types of reinforced concrete 2D and 3D frames subject to seismic sequences. Damage accumulation of frame members was noticed after the analyses, confirming the increase of ductility demand due to repeated shakings. Reinforced concrete structures were also investigated by Hosseinpour and Abdelnaby (2017a, b) who derived fragility curves for different limit states of RC frames subject to multiple seismic sequences. Raghunandan et al. (2015) carried out incremental dynamic analyses of intact and pre-damaged frames providing also fragility curves. The authors recognized that the dependence of the residual capacity to resist aftershocks was strictly correlated with the damage level induced by the mainshock event. Other authors addressed the behaviour of steel structures under mainshock/aftershock sequences. Among these Li et al. (2014) investigated a four storey moment resisting steel frame performing incremental dynamic analyses after different levels of damage induced by the mainshock. Fragility curves associated, confirmed an increase of the collapse probability as the mainshock induced damage level increased. A reliability-based robustness assessment of steel frames structures subject to post-mainshock cascading events was finally proposed by Ribeiro et al. (2014).

The aforementioned studies, besides other aspects, highlighted that the capacity of a structure to survive aftershock earthquakes depends on the residual strength and displacement capacity at the end of the main event. However, previous studies refer the behaviour of RC or steel bare frames, neglecting the influence of masonry infill walls, although it is well known that infills radically modify seismic response of frame structures subject to seismic events. Masonry infills contribution to seismic performance of frame structures has been widely investigated in the past. The main conclusion drawn, refer that infills can effectively reduce seismic damage as a consequence of the reduced displacement demand and strength increment (Dolšek and Fajfar 2008; Cavaleri et al. 2017). On the other hand infill-frame interaction may also lead to local failures in proximity of the ends of columns and of the joints (Cavaleri and Di Trapani 2015; Celarec and Dolšek 2013). Recent literature reviews in the field (Di Trapani et al. 2015; Asteris et al. 2017) express growing need for accurate modelling of infilled frames to perform reliable seismic assessment of new and existing constructions (Asteris et al. 2015; Pantò et al. 2017; Cavaleri et al. 2012, 2014; Campione et al. 2015, 2016, 2017; Di Trapani et al. 2018a, b).

Despite the huge amount of modelling proposals, the most effective way to model masonry infills in frame structures when performing repeated seismic simulations, is using equivalent diagonal struts replacing infills (e.g. Mainstone 1974; Cavaleri and Di Trapani 2014; Asteris et al. 2016). This approach accounts inelastic behaviour of infills with relatively low computational effort. Additional shear demand on columns can be evaluated through simplified formulas based on correlations (Di Trapani et al. 2018a, b) or simplified equilibrium approaches.

Considering the aforementioned issues, this paper presents an assessment framework specifically thought to assess the influence of masonry infill walls on the seismic fragility of reinforced concrete structures subjected to single or sequential (mainshock/aftershock) seismic events. A double incremental dynamic analysis (D-IDA) approach is used to carry out the assessment of bare and in filled frames. D-IDA ground motion signals are composed of mainshocks with fixed intensity and variable aftershocks each time scaled in amplitude. IDAs are then repeated changing the intensity of the mainshock in such a way that scaling in amplitude is carried out both on mainshock and aftershocks. A reference structure, consisting in a real prototype 4-storey reinforced concrete frame, has been chosen to perform numerical simulations. The proposed framework points out a proper definition of limit states and intensity measures to consider for a reliable assessment.

Results provide fragility curves of bare and infilled frame with different levels of mainshock intensity. Residual capacity and aftershock loss diagrams, illustrating the reduction of median collapse intensity as a function of mainshock intensity, are finally provided for bare and infilled frames.

2 Mainshock/aftershock fragility assessment framework

2.1 Double incremental dynamic analysis with mainshock/aftershock ground motions

Incremental Dynamic Analysis (IDA) (Vamvatsikos and Cornell 2002) has been widely employed during last years as reference method for the probabilistic assessment of seismic performance of structures. IDA consists in subjecting the structure under investigation to a set of design spectrum compatible ground motions, which are scaled in amplitude up to the achievement of a selected limit state. For each accelerogram, a nonlinear time history analysis is run at every intensity level. The achievement of a limit state can be conventional (e.g. achievement of a specified drift threshold) or can be actually monitored on structural elements at each stage of the analysis. Incremental dynamic analysis is generally thought to assess undamaged structures undergoing a seismic event for the first time. The standard IDA procedure is here modified by performing a double incremental dynamic analysis in order to consider different mainshock/aftershock combinations. The steps to carry out D-IDA provide first defining ground motions as an assemblage of two signals, namely the mainshock and the aftershock, interspersed with a decay time sufficient to bring the structure back to static condition. Mainshock and aftershock ground motions are taken from the same set of spectrum compatible accelerograms. Incremental dynamic analysis is performed using a mainshock ground motion having fixed intensity, each time combined with aftershocks scaled in amplitude. A set of at least 30 aftershock accelerograms is suggested to adequately consider the uncertainty associated with ground motion variability. IDAs are then repeated by changing the mainshock intensity and associating the same set of scaled aftershock ground motions. The double scaling of both mainshock and aftershocks allows deriving fragility curves depending on mainshock intensity, and can be used to define residual capacity diagrams reporting the average residual capacity of a structure as a function of mainshock intensity. A sample of the ground motion composition is illustrated Fig. 1.

Maximum interstorey drifts, and peak ground acceleration (PGA) are selected as damage measure (DM) and intensity measure (IM) respectively. The choice of PGA instead of spectral acceleration ($S_e(T_1)$) is justified by two main considerations. Firstly, the fundamental period of vibration (T_1) of undamaged and damaged structure is different. Consequently, using a unique value of T_1 is unsuitable to compare results from intact and damaged structures. Further, the use of PGA allows comparing results from bare and infilled frame structures, which would be not possible with a unique $S_e(T_1)$ value because of the really different vibration periods.

2.2 Definition of collapse limits states on D-IDA curves

The achievement of actual ultimate chord-rotation and ultimate shear capacity of columns are adopted as collapse limit states. The common assumption (also suggested in FEMA technical code) to consider the achievement of 2% interstorey drift as collapse limit state for reinforced concrete structures cannot be considered reliable for infilled frames. In fact infills behave as compression bracings, which increase, at the same time, base shear and base moment. This results in a significant axial force excursion on columns and, consequently, in a large variation of ultimate chord rotation capacity, especially of external columns. In order to consider the coupling between axial force and chord rotation, analytical axial-force/chord-rotation domains (Fig. 2) are defined for the base cross-section of columns. Ultimate chord rotations are evaluated by means of Eurocode 8 (2004) formulas, which depend on both ultimate and yielding curvatures. The latter are determined through a fiber section analysis of each cross-section for each axial force level. Scattered axial-force/chord rotation (N_i-Θ_i) values are fitted with a

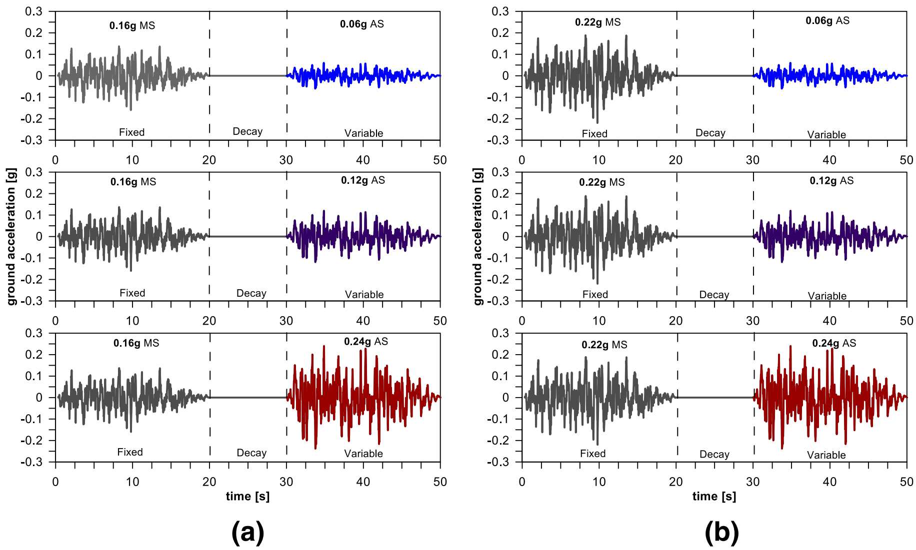

Fig. 1 Composition of ground motion signals for double incremental dynamic analysis: **a** fixed 0.16 g PGA mainshock with scaled aftershocks; **b** fixed 0.22 g PGA mainshock with scaled aftershocks

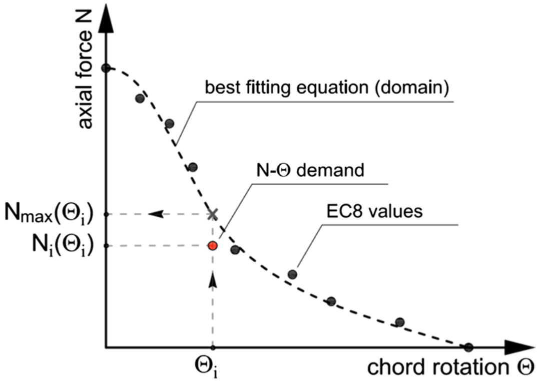

Fig. 2 Axial force–chord rotation domains

N(Θ) analytical equation, which is used to determine the maximum axial force ($N_{max}(\Theta_i)$) that can be achieved at the generic rotation Θ_i (Fig. 2). The limit state is reached when the axial force value $N_i(\Theta_i)$ associated with the generic chord-rotation Θ_i exceeds the maximum value $N_{max}(\Theta_i)$, namely:

$$N_i(\Theta_i) \leq N_{\max}(\Theta_i) \tag{1}$$

Masonry infills may also induce shear collapse of frames because of excess of shear demand at the end of columns (Cavaleri and Di Trapani 2015; Jeon et al. 2015). The actual shear demand on columns can be directly evaluated by using a multi-strut macro-model for the infill (e.g. El-Dakhakhni et al. 2003; Jeon et al. 2015) or, in case of single concentric struts, can be estimated by using the following expression based on simple equilibrium considerations:

$$V_{C,\inf} = P_{str}\cos\alpha - \mu P_{str}\sin\alpha \tag{2}$$

where, referring to Fig. 3, $V_{C,inf}$ is the additional shear demand actually transferred from the infill to the column, P_{str} the current value of the axial force acting on the equivalent strut, α the angle of inclination of the strut with respect to horizontal direction and μ the friction coefficient associated with the infill-mortar-frame interface. Shear limit state is expressed by the following condition:

$$V_{C,d} = V_{C,fr} + V_{C,\inf} \leq V_{Rd} \tag{3}$$

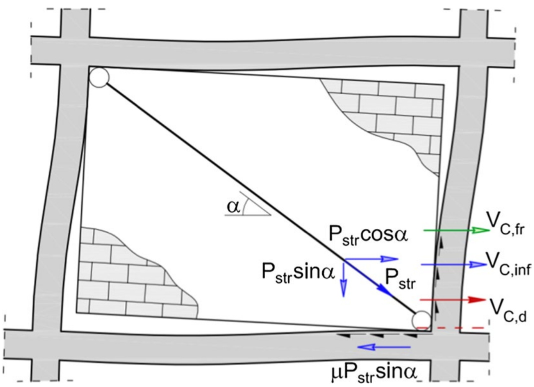

Fig. 3 Simplified scheme for the determination of actual shear demand on columns for an infilled frame

where $V_{C,fr}$ is shear force evaluated on the frame (in any section of a column), and V_{Rd}, the shear capacity of the column.

2.3 Derivation of fragility curves and aftershock residual capacity diagrams

Fragility curves express the probability of exceeding a limit state as a function of the intensity measure selected. Fragility curves are here referred to the distribution of PGA in correspondence of collapse limit states, which is generally a lognormal distribution (Fig. 4).

A lognormal cumulative distribution function is then used to analytically define fragility curves. The latter provides the probability of exceeding the collapse limit state (DM_{CO}) as a function of PGA. Fragility curves are analytically expressed as:

$$P(DM \geq DM_{CO}) = \Phi\left(\frac{\ln X - \mu_{\ln X}}{\sigma_{\ln X}}\right) \tag{4}$$

where Φ is the standard cumulative distribution function, lnX is the natural logarithm of the variable X (collapse PGA) and $\mu_{\ln X}$ and $\sigma_{\ln X}$ are the mean and the standard deviation of the natural logarithms of the distribution of X respectively. Fragility curves obtained analytically are then compared with discrete cumulative distribution data from IDA in order to test their reliability. Assessment of seismic fragility will provide collapse probability of bare and infilled frames subject to single seismic events and to mainshock/aftershock sequences.

The adopted double IDA procedure allows defining residual capacity domains and aftershock loss diagrams. The first reports collapse PGA at different probabilities of exceeding (e.g. 16, 50 and 84%) as a function of increasing mainshock PGA levels (Fig. 5a). The initial point of the diagram (mainshock PGA equal to zero) represents the undamaged condition. The last point is, obviously, associated with the collapse in the mainshock (no residual capacity against aftershocks). The second diagram (Fig. 5b) represents capacity losses with respect to the undamaged condition as a function of mainshock intensity. Vertical axis values are obtained as ratio between average aftershock collapse PGA and average collapse PGA at the undamaged condition.

Fig. 4 Limit states distribution on IDA curves

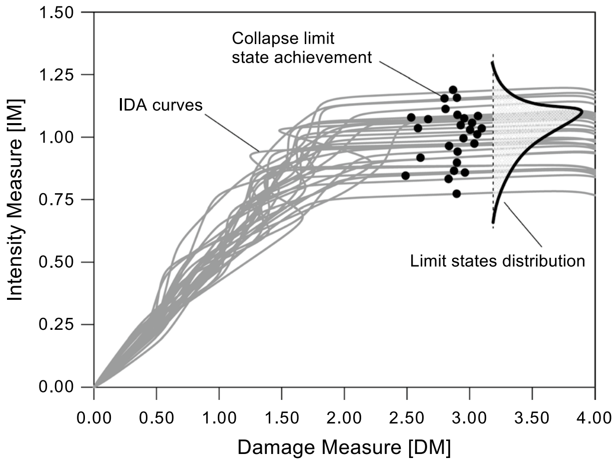

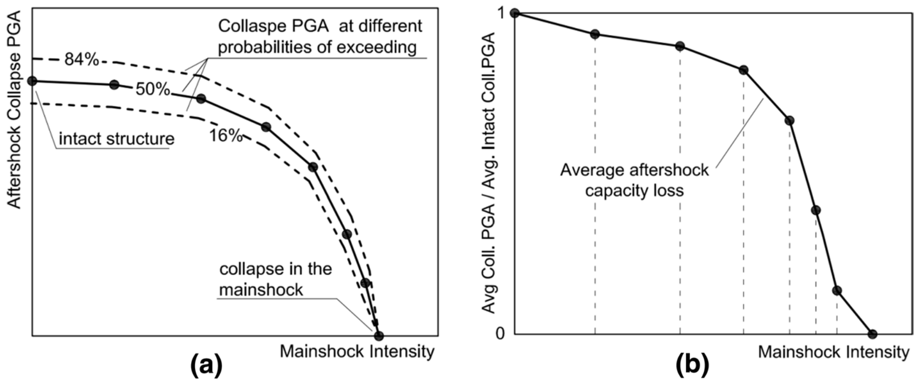

Fig. 5 Residual capacity diagrams: **a** residual capacity domains; **b** average aftershock capacity loss diagram

This diagrams typology, besides assessing residual capacity, allows comparing performance of different structures or different structural systems (e.g. bare and infilled frames) to mainshock/aftershock sequences and can be used for both assessment and design purposes.

3 Reference structure details and modelling

3.1 Geometric and material details

In order to test the proposed approach for assessing mainshock/aftershock fragility of existing infilled frame structures, a reference case study is selected to be representative of typical RC buildings realized from 1960s to the 1980s in Southern Europe. The reference structure is a full scale prototype building tested at ELSA laboratory (Carvalho and Coelho 2001). The same structure was adopted as reference in more recent numerical studies (e.g. Dolšek and Fajfar 2008; Pantò et al. 2017). The original experimental campaign consisted of several shake table tests of two identical four-storey three-bay frame specimens not provided with seismic details. One of the two specimen was a bare frame while the other was the same frame arranged with hollowed clay masonry infills walls with openings. The geometry of RC frames elements, reinforcement details and material properties was typical of non-seismically designed buildings of that period. Geometric and material details are shown in Fig. 6.

The average compressive strength of concrete and steel reinforcement were $f_c = 16.3$ MPa and $f_y = 343.6$ MPa respectively. The very low strength of concrete is consistent with typical results from core drillings of 1960–1980 reinforced concrete building, and represents a bad arrangement and design of concrete. The infilled frame was arranged with clay hollow masonry blocks having a thickness of 120 mm without plaster and 200 mm considering plaster. The original infilled specimens had window and door openings in two of the three bays. Results of the experimental tests on masonry wallets have been taken from data reported by Varum (2003). A summary is provided in Table 1.

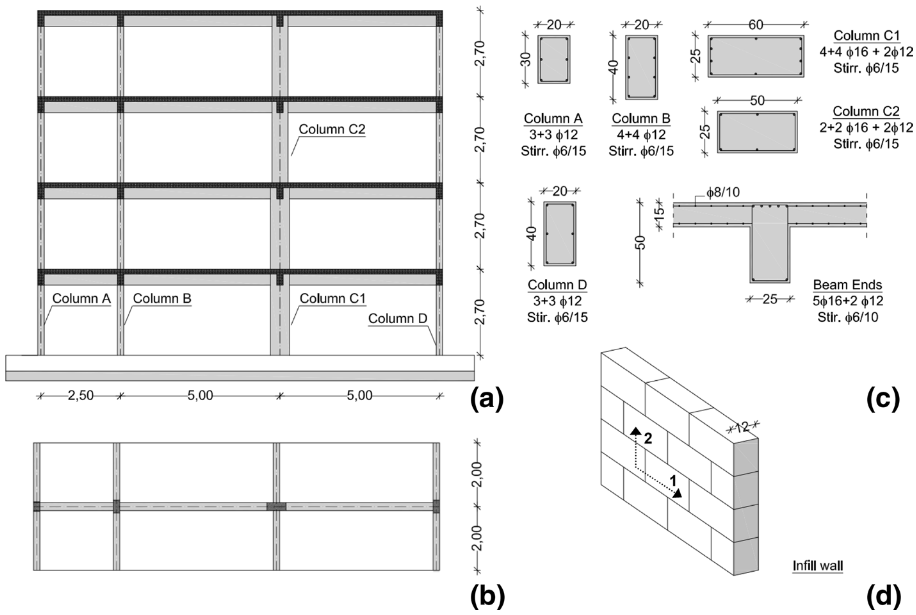

Fig. 6 Details of the reference structure: **a** geometric details in elevation (m); **b** geometric details in plan (m); **c** cross-section details (cm); **d** infill wall geometric details and reference axes (cm)

3.2 Modelling of frame and infills

Bare and infilled frames were modelled as 2D frames using the OpenSees (McKenna et al. 2000) software platform. One-dimensional fiber-section beam elements were used to model frames. Infills were modelled with a pair of concentric equivalent struts. The latter are fiber-section trusses resisting only in compression. Vertical loads, consistently with actual data, were 9.1 kN/m^2 (36.4 kN/m on beams) for the first 3 floors and 8.0 kN/m^2 (32 kN/m on beams) for the last floor. Masses were proportionally distributed on the floor nodes.

Beams and columns were modelled with the nonlinear beam/column element implemented in OpenSees. The fiber cross-sections of RC elements were assembled by assigning different uniaxial stress–strain laws to concrete core and cover fibers in order to account for stirrups confinement. The Concrete02 model was used for concrete fibers (Fig. 7). Confined and unconfined stress–strain curves (parameters f_{c0}, ε_{c0}, f_{cu}, ε_{cu}; f_{cc0}, ε_{cc0}, f_{ccu}, ε_{ccu}) were evaluated according to local reinforcement details. Parameters used for concrete in tensions were $f_t = 2.0$ MPa (tensile strength) and $E_t = 1500$ MPa (tension softening stiffness). Steel rebars were modelled as spread layers with the Steel02 material model. The elastic Young's modulus was $E_s = 210{,}000$, while the hardening ratio was $b = 0.01$.

Differently from the actual specimen, the model was considered to have solid infills. Infill were replaced by pair of compression only concentric diagonal equivalent struts (Fig. 8). The diagonals consisted of fiber-section trusses governed by the stress–strain law of fibers. The identification of diagonals was carried out using the model proposed by Asteris et al. (2016) for determining the cross-section width, in combination with the recently developed approach by Di Trapani et al. (2018a, b) for the definition of stress–strain constitutive law of fibers.

Table 1 Results of experimental tests on masonry wallets (Varum 2003)

Compression parallel to bed joints (1) f_{m1} (MPa)	Compression orthogonal to bed joints (2) f_{m2} (MPa)	Diagonal compressive strength f_{vm} (MPa)	Compression parallel to bed joints (1) E_{m1} (MPa)	Compression orthogonal to bed joints (2) E_{m2} (MPa)	Shear modulus G (MPa)
3.97	1.11	0.23	1873	991	1171

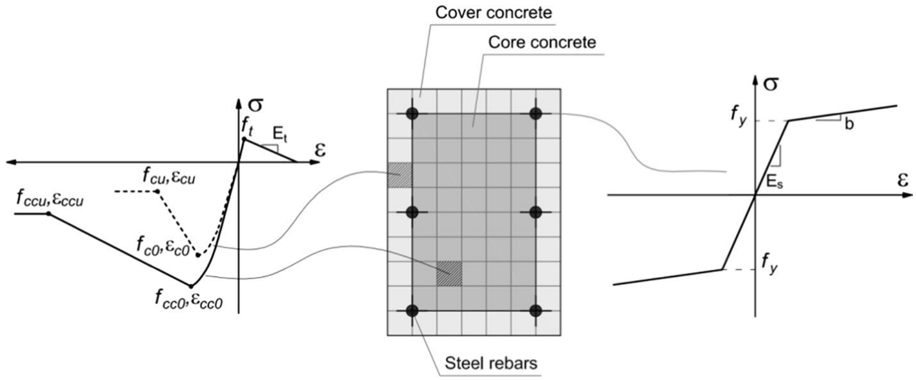

Fig. 7 Definition of the fiber cross-section of RC elements and associated uniaxial stress–strain models of materials

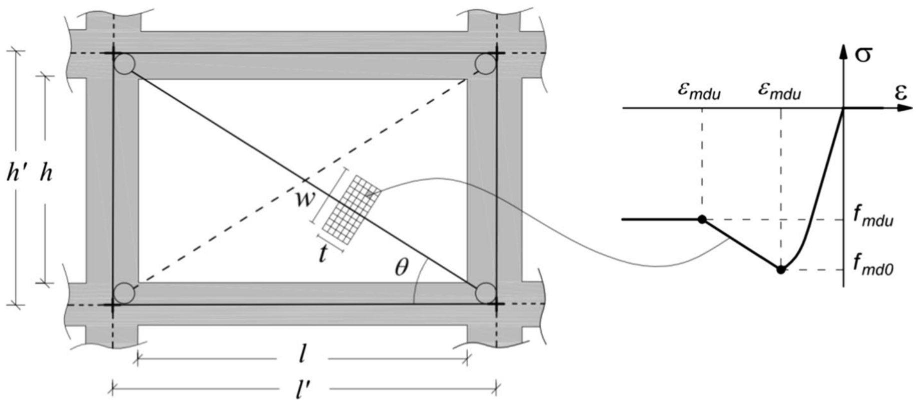

Fig. 8 Equivalent struts fiber-section modelling

This method provides a concrete type stress–strain model (parabolic with linear softening) (Fig. 8). The stress–strain curve is defined by evaluating four parameters, peak stress f_{md0}, ultimate stress f_{mdu}, peak strain ε_{md0}, and ultimate strain ε_{mdu}, which are obtained using the following semi-empirical equations:

$$f_{md0} = 26.9\tilde{f}_m \cdot \alpha^{-0.287} \tag{5}$$

$$f_{mdu} = f_{md0}(0.043\beta - 0.06) \tag{6}$$

$$\varepsilon_{md0} = 3.024 \cdot \varepsilon_{m0} \cdot \gamma^{0.347} \tag{7}$$

$$\varepsilon_{mdu} = 0.0184 \cdot \varepsilon_{md0} \cdot \delta^{-1.166} \tag{8}$$

where parameters α, , and δ are directly linked to the geometrical and mechanical features of each infilled frame by the following correlation laws:

$$\alpha = \frac{\tilde{f}_m^2 \cdot w \cdot t}{\left(f_{vm} + \mu\sigma_n\right)^{0.2}(l/h) \cdot \lambda^{*0.2}} \tag{9}$$

$$\beta = \frac{f_{md0}^{0.7} \cdot w \cdot t}{\tilde{E}_m^{0.2} d} \tag{10}$$

$$\gamma = \left(\frac{f_{mdu}^2}{f_{md0}}\right)\left(\frac{E_c}{\tilde{E}_m^{1.5}}\right) \tag{11}$$

$$\delta = \tilde{E}_m^{0.20} \cdot \varepsilon_{md0} \tag{12}$$

In previous equations ε_{m0} is the peak strain of masonry in compression, conventionally assumed equal to 0.0015, $\tilde{f}_m$ and $\tilde{E}_m$ are conventional compressive strength and elastic modulus of masonry, which are used to summarize the different strength and stiffness of masonry along the main orthogonal directions, assuming the expressions:

$$\tilde{f}_m = \sqrt{f_{m1} \cdot f_{m2}}; \quad \tilde{E}_m = \sqrt{E_{m1} \cdot E_{m2}} \tag{13}$$

In Eq. (13) f_{m1}, f_{m2}, E_{m1}, E_{m2} are the strengths and the elastic moduli along the two orthogonal directions, σ_n is the average normal stress on the infill due to vertical loads (proportional to the vertical stiffness ratio between infills and columns), E_c is the elastic Young's modulus of concrete, d is the diagonal length of the strut, l and h are the length and the height of the infill, t is the thickness of the infill, assumed to be equal to the actual net thickness (120 mm), w is the width of the strut, evaluates, as previously mentioned, according to the procedure by Asteris et al. (2016). The hysteretic behaviour of the struts is ruled by the parameter λ, which regulates the ratio between elastic and inelastic slopes of the unloading branches. The parameter λ is set equal to 0.07 for the equivalents struts and 0.1 for the concrete elements. The identification data for the equivalent struts of the reference structure are shown in Table 2.

Since the model is defined with using equivalent concentric struts, and uniaxial stress–strain constituive models without strain limits, the achievement shear and chord rotation limit states is not expressly detected during the analyses, but in the post-processing phase by applying Eqs. (1) and (3) to resulting data. For the current case, shear strength of columns (V_{Rd}) is evaluated as provided by the Italian Technical Code (D.M. LL. PP 14.01.2008) for existing RC buildings as the sum of shear reinforcement resistance contribution and concrete resistance contribution evaluated considering the case of RC members without shear reinforcement.

4 Double incremental dynamic analysis program

Bare frame (BF) and infilled frame (IF) models were subject to double incremental dynamic analysis. Both mainshock and aftershocks were scaled in order to evaluate aftershock fragility curves for each given mainshock intensity. The cases of no pre-damage (intact structures) were also considered by carrying out a standard IDA procedure. The double scaling of mainshock and aftershock allowed also defining the residual capacity diagrams. The target spectrum was defined according to the seismic hazard of L'Aquila (Italy), considering a return period of 1950 years. A set of 30 artificial spectrum compatible ground motions of 15 s duration was generated using the SIMQKE-I software platform (Vanmarcke et al. 1976). The ground motion spectra set is shown in Fig. 9 together with

Table 2 Geometrical and mechanical Identification parameters of the equivalent struts

Infill type	Floor no.#	f_{vm} (MPa)	$\tilde{f}_m$ (MPa)	$\tilde{E}_m$ (MPa)	w (mm)	t (mm)	f_{vm} (MPa)	$\tilde{f}_m$ (MPa)	f_{md0} (MPa)	f_{mdu} (MPa)	ε_{md0} (–)	ε_{mdu} (–)	λ (–)
Between col. A–B	1	0.23	2.09	1362	1146.3	120	0.23	2.09	1.11	0.38	0.0018	0.0097	0.07
Between col. B-C/C–D	1	0.23	2.09	1362	1382.9	120	0.23	2.09	1.19	0.33	0.0016	0.0100	0.07
Between col. A–B	2	0.23	2.09	1362	1127.9	120	0.23	2.09	1.11	0.37	0.0018	0.0098	0.07
Between col. B–C/C–D	2	0.23	2.09	1362	1269.8	120	0.23	2.09	1.22	0.31	0.0015	0.0100	0.07
Between col. A–B	3	0.23	2.09	1362	1109.7	120	0.23	2.09	1.10	0.36	0.0018	0.0098	0.07
Between Col. B–C/C–D	3	0.23	2.09	1362	1165.2	120	0.23	2.09	1.24	0.28	0.0014	0.0101	0.07
Between col. A–B	4	0.23	2.09	1362	1091.5	120	0.23	2.09	1.10	0.35	0.0017	0.0098	0.07
Between col. B–C/C–D	4	0.23	2.09	1362	1068.5	120	0.23	2.09	1.26	0.26	0.0013	0.0102	0.07

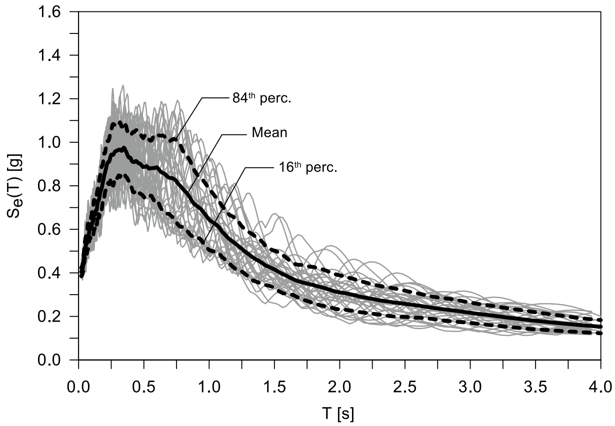

Fig. 9 Selected ground motion spectra

16th, 50th and 84th percentile spectra. The choice of using artificial accelerograms simply depended on the possibility to set a fixed duration of the signals. This makde easier the definition of the different mainshock/aftershock combinations. Expected results are more likely less scattered with respect to those obtainable form real ground motion record set, but the overall assessment is reasonably supposed to be not substantially different. Several trial IDAs were carried out in order to define the range of PGA scaling intensities to adopt for mainshock and aftershocks. In detail MS intensity scaling levels were defined after performing a single record IDA of bare and infilled frame with the MS ground motion to determine mainshock collapse PGA. Selected mainshock intensities are a percentage of detected collapse PGA (0.19 g and 0.32 g for bare and infilled frame respectively). Bare frames were subjected to the cases of no pre-damage (intact structure) (0%), 0.10 g (53%) and 0.16 g (85%) mainshocks. The following aftershock accelerograms were scaled to 13 PGA levels ranging between 0.01 g and 0.22 g PGA (Table 3). For the infilled frame a larger scaling set was used. In fact, the cases of intact structures (0%), 0.10 g (32%), 0.16 g (50%), 0.22 g (69%) and 0.26 g (81%) mainshock were considered. The following aftershocks had 18 PGA levels ranging between 0.01 and 0.32 g.

5 Analysis results

5.1 Standard and double IDA results for bare and infilled frames

IDA curves of bare and infilled frames showed significant differences both for intact and damaged states (Figs. 10, 11). The presence of masonry infills resulted in a noticeable increase of the average PGA at which collapse limit state was achieved (+68% for intact infilled frame with respect to bare case). This is due to the strong stiffening action exerted by the infills which results in an increase of seismic intensity level necessary to induce limit chord rotations of RC frame columns. It should be also observed that such strength increment was possible since frame members were able to support the additional shear demand arising. As a secondary effect, the presence of the masonry infills resulted to play a fundamental role on the residual capacity to resist aftershocks. IDA curves reported in Fig. 10, in fact, show that average collapse PGA of bare frame rapidly decreased with an

Table 3 Double incremental dynamic analysis program

Bare frame		Infilled frame	
Mainshock PGA (g)	Aftershocks PGA (g)	Mainshock PGA (g)	Aftershocks PGA (g)
(–) Intact	0.01, 0.02, 0.03, 0.04, 0.06, 0.08, 0.10, 0.12, 0.14, 0.16, 0.18, 0.20, 0.22	(–) Intact	0.01, 0.02, 0. 03, 0.04, 0.06, 0.08, 0.10, 0.12, 0.14, 0.16, 0.18, 0.20, 0.22, 0.24, 0.26, 0.28, 0.30, 0.32
0.10	0.01, 0.02, 0. 03, 0.04, 0.06, 0.08, 0.10, 0.12, 0.14, 0.16, 0.18, 0.20, 0.22	0.10	0.01, 0.02, 0. 03, 0.04, 0.06, 0.08, 0.10, 0.12, 0.14, 0.16, 0.18, 0.20, 0.22, 0.24, 0.26, 0.28, 0.30, 0.32
0.16	0.01, 0.02, 0. 03, 0.04, 0.06, 0.08, 0.10, 0.12, 0.14, 0.16, 0.18, 0.20, 0.22	0.16	0.01, 0.02, 0. 03, 0.04, 0.06, 0.08, 0.10, 0.12, 0.14, 0.16, 0.18, 0.20, 0.22, 0.24, 0.26, 0.28, 0.30, 0.32
		0.22	0.01, 0.02, 0. 03, 0.04, 0.06, 0.08, 0.10, 0.12, 0.14, 0.16, 0.18, 0.20, 0.22, 0.24, 0.26, 0.28, 0.30, 0.32
		0.26	0.01, 0.02, 0. 03, 0.04, 0.06, 0.08, 0.10, 0.12, 0.14, 0.16, 0.18, 0.20, 0.22, 0.24, 0.26, 0.28, 0.30, 0.32

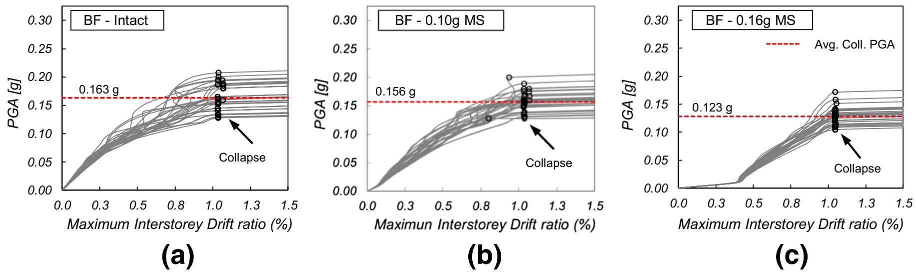

Fig. 10 IDA and D-IDA curves of bare frame and collapse limit state points: **a** intact structure; **b** with prior 0.10 g mainshock; **c** with prior 0.16 g mainshock

increase of the mainshock intensity. Residual mainshock damage was significant for the largest MS intensity (0.4% residual drift), as it can be observed form Fig. 10c. Bare fame collapsed in the mainshock for MS intensities larger than 0.16 g.

D-IDA curves of infilled frame show that average collapse PGA was substantially not reduced up to a MS intensity of 0.16 g. Larger mainshock intensities (0.22 g and 0.26 g) caused more evident residual drifts (Fig. 11d, e) which corresponded to more scattered, and averagely lower, PGA collapse values. The procedure adopted to evaluate ultimate chord-rotation limit states as a function of the actual axial force acting on a column was fundamental to get reliable results for the infilled frame structure. In fact, stiffening action due to the infills resulted in a significant overall overturning effect. External columns were subjected to large axial force excursions (up to three times) with respect to the bare frame case (Fig. 12a, d), alternating also compression and tension.

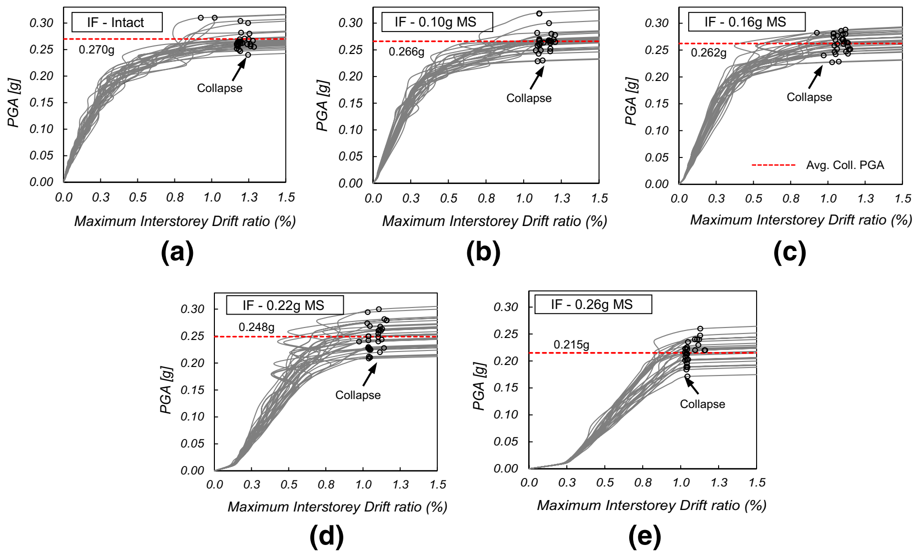

Fig. 11 IDA and D-IDA curves of infilled frame and collapse limit state points: **a** Intact structure; **b** with prior 0.10 g mainshock; **c** with prior 0.16 g mainshock; **d** with prior 0.22 g mainshock; **e** with prior 0.26 g mainshock

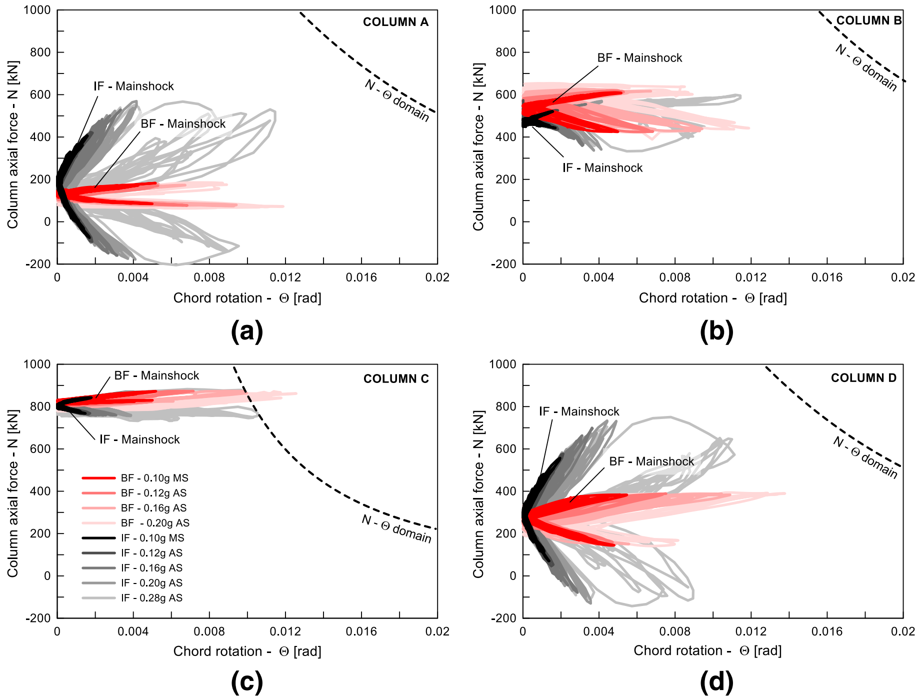

Fig. 12 Axial force–cord rotation trajectories of the base cross-sections of bare and infilled frames subjected to 0.10 g PGA mainshock and increasing aftershock levels: **a** column A; **b** column B; **c** column C; **d** column D

In Fig. 12, the different axial-force/chord-rotation responses of bare and infilled frame structure 1st storey columns subject to the same mainshock (0.10 g PGA) and one aftershock ground motion of increasing intensity can be observed in detail. Axial-force (N)/chord-rotation (Θ) limit curves are also reported in Fig. 12. N-Θ trajectories at the base cross-sections follow substantially different paths for bare and infilled frame cases. This is more evident for columns A and D, where the column axial force excursion is maximum. The effect of masonry infills in delaying aftershock collapse results also evident by observing bare and infilled frame N-Θ responses to the same AS and MS intensities. Collapse is achieved in column C (Fig. 12c) both for bare and infilled frame, in correspondence of 0.16 g and 0.28 g aftershock PGA respectively with an overall capacity increase of + 75%. The overall structural behaviour clearly reflects results discussed up to here. Figures 13 and 14 show base-shear versus first interstorey displacement response curves of bare and infilled frame subjected to increasing mainshock/aftershock sequences. By comparing bare and infilled frame responses at the first two MS/AS sequences (Figs. 13a, b and 14a, b) it can be observed that aftershock inelastic demand (and hence damage) associated with the infilled frame is significantly lower. The two MS ground motions (0.10 g and 0.16 g) resulted in almost linear response from the infilled frame, conversely to bare frame which has shown significant inelastic excursion especially with 0.16 g mainshock. Considering the 0.22 g AS, the displacement demand reduction of the infilled frame with respect to the bare frame, was − 67% and − 58%, respectively after 0.10 g and 0.16 g MS.

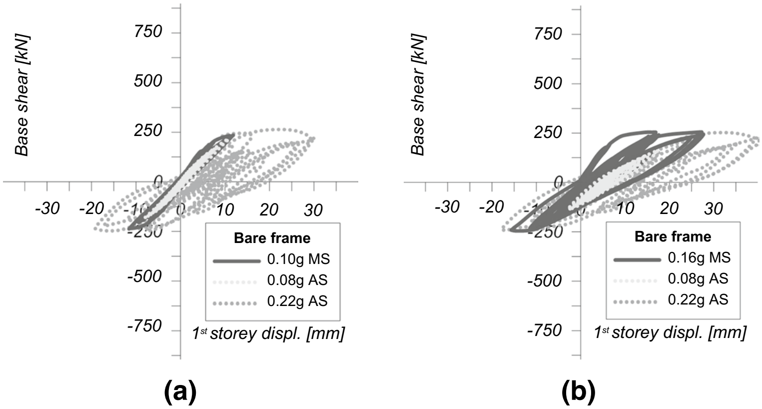

Fig. 13 Base shear versus 1st storey displacement aftershock response of bare frame with a mainshock of increasing intensity: **a** 0.10 g mainshock; **b** 0.16 g mainshock

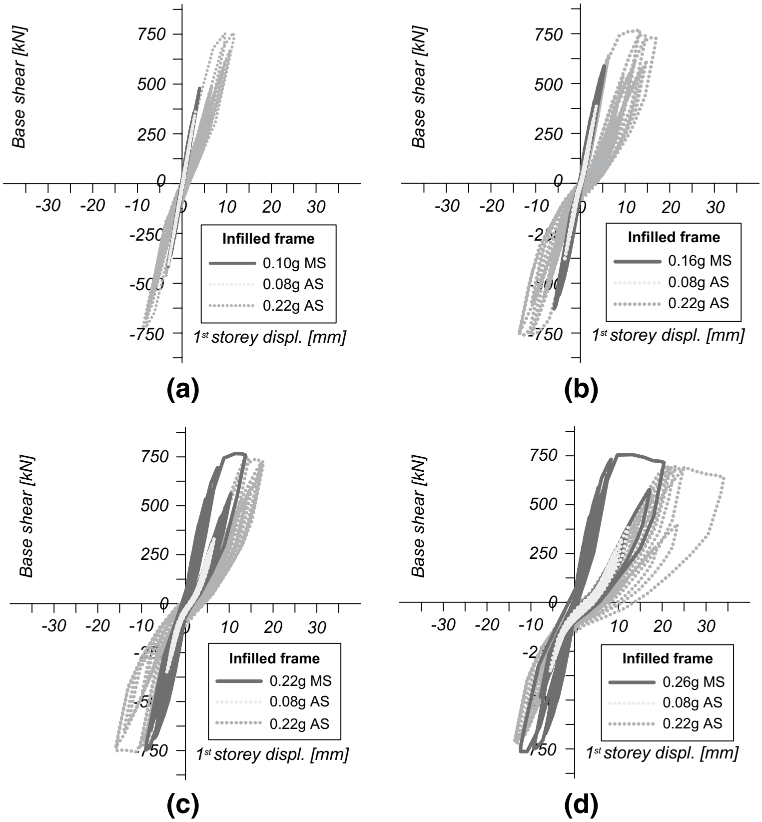

Fig. 14 Base shear versus 1st storey displacement aftershock response of infilled frame with a mainshock of increasing intensity: **a** 0.10g mainshock; **b** 0.16g mainshock; **c** 0.22g mainshock; **d** 0.26g mainshock

Appreciable structural damage could be detected for the infilled frame starting from 0.22 g MS, where the first storey infills achieved peak load. Aftershock force–displacement curves (Fig. 14c, d) showed significant reduction of initial stiffness due to the crushing of infills. However, maximum interstorey displacements achieved were still lower than those of bare frame for the first two MS/AS sequences.

5.2 Fragility curves and aftershock residual capacity

Both analytical and discrete fragility curves are shown in Fig. 15. While the former are defined by using Eq. (4) and depend on means and standard deviations of collapse peak ground accelerations natural logarithms, the second represent the actual cumulative distributions resulting from IDAs. The agreement between analytical and discrete fragility curves gives confirmation of the reliability of the lognormal distribution provided by Eq. (4).

Results discussed in the previous section can be quantitatively assessed through fragility curves. Focusing on intact bare and infilled frame (solid lines), it is noteworthy observing that fragility curve of infilled frame is significantly shifted on the right with respect to bare one, confirming a significant reduction of seismic fragility due to the influence of infills. The average collapse probability is achieved in correspondence of 0.16 g PGA for the bare frame and 0.27 g PGA for the infilled frame, with an overall increase of 68%. At the same time it can be observed that collapse probability of 100% of the bare structure is associated with a PGA of about 0.23 g, corresponding to 2.5% of collapse probability for the infilled frame.

Aftershock IDA curves, obtained with double-IDA show to be dependent on the mainshock intensity. Aftershock fragility obviously increases with increasing mainshock PGA. However this occurs in a different way for the cases of bare and infilled frame. Bare frame fragility curves display rapid and significant shifting on the left with respect to the intact curve for 0.10 g and 0.16 g mainshocks. The same mainshocks provide only moderate aftershock fragility increases for the infilled frame. Noticeable fragility increase of the infilled frame was recognized only after 0.22 g and 0.26 g mainshocks. However, it is

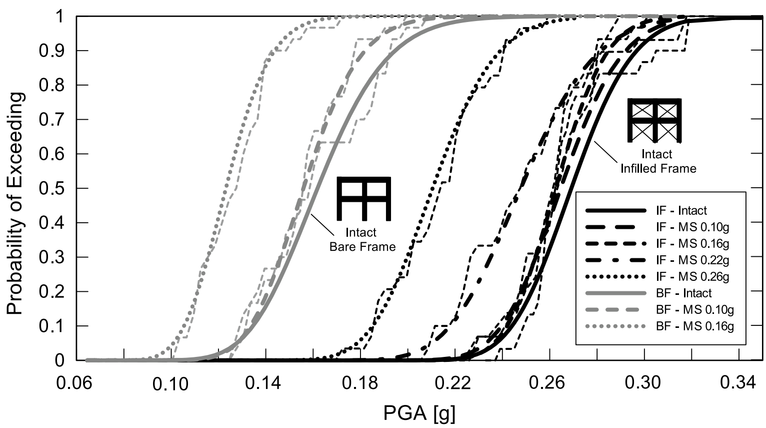

Fig. 15 Intact and aftershock fragility curves of bare and infilled frames (analytical curves and cumulative distributions from IDA results)

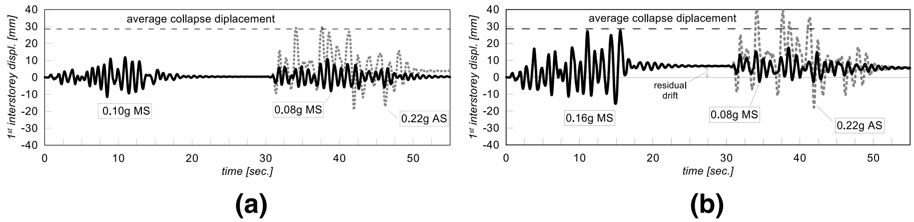

Fig. 16 Mainshock/aftershock time versus displacement response of bare frame: **a** 0.10 g MS; **b** 0.16 g MS

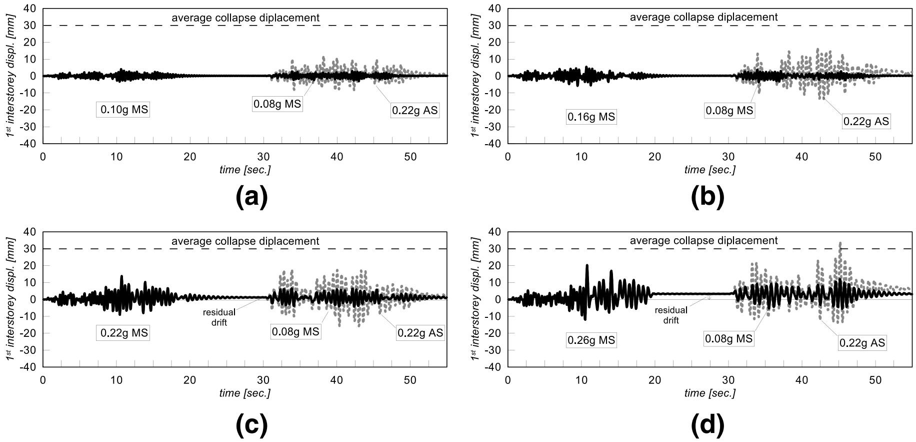

Fig. 17 Mainshock/Aftershock time versus displacement response of infilled frame: **a** 0.10 g MS; **b** 0.16 g MS; **c** 0.22 g MS; **d** 0.26 g MS

noteworthy observing that PGA corresponding to the average collapse probability of the infilled frame with 0.26 g mainshock PGA (0.21 g) still remained 30% larger than intact bare frame average collapse PGA (0.16 g).

Fragility increases were not directly proportional to mainshock intensity. In fact both for bare and infilled frames the aftershock capacity is significantly reduced only beyond a MS intensity inducing noticeable residual interstorey drift. This is evident by observing Figs. 16 and 17, which show time versus interstorey displacement response of bare and infilled frames subject to increasing mainshocks and aftershocks. Displacement peaks undergo large amplification only for the cases in which considerable residual drifts occur after the mainshock.

Results from double incremental dynamic analysis can be summarized to define residual capacity domains and aftershock loss diagrams. The former (Fig. 18a) represent the average capacity (in terms of collapse PGA) as a function of mainshock intensity experienced by the structure. The collapse PGA record-to-record variability is considered by representing also 16% and 84% percentiles curves. The larger residual capacity against aftershocks exhibited by infilled frames can be graphically observed from the domains in Fig. 18a. The curves also clearly highlight that bare frame rapidly loses capacity to resist further earthquakes after a certain mainshock intensity is achieved. This trend is significantly delayed in the case of the infilled frame, which has shown to maintain almost the undamaged capacity

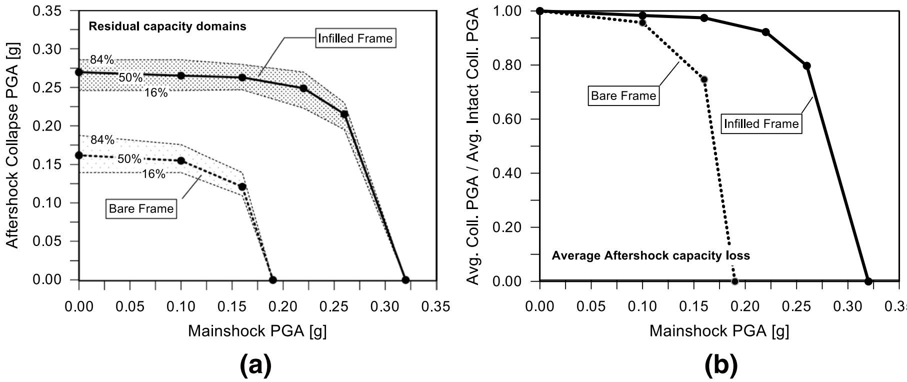

Fig. 18 Residual capacity diagrams: **a** residual capacity domains; **b** aftershock capacity loss diagrams

even beyond mainshock intensities causing 100% collapse probability for the bare structure. Aftershock capacity loss is assessed by diagrams in Fig. 18b, showing the different normalized capacity losses of bare and infilled frames in terms of average collapse PGA. Residual capacity loss is almost the same for bare and infilled frame up to a MS intensity of 0.10 PGA. Beyond this point, bare frame loss curve significantly diverges from the infilled one; achieving total residual capacity loss at 0.19 g MS (collapse in the mainshock). In correspondence of the same point the bare frame maintains 95% of the intact capacity. The total residual capacity loss was achieved at 0.315 g PGA for the infilled frame, resulting in an increase of +66% with respect to the bare case. Results allow concluding that masonry infills provide significant additional capacity to intact and damaged structures. Capacity increment is so large to assert that infill walls can be fundamental to the earthquake survival of structures both in mainshocks and aftershocks. It should be anyway observed that such positive contribution of infills is possible if local shear failure of columns and joints due to the infill-frame interaction does not occur. Next section will present results for the same structures assuming to increase stirrups spacing of columns, in order to induce anticipated shear collapse.

6 Double IDA and fragility assessment of in infilled frames with shear failure

In order to assess the dependence of infilled frames response on the failure mode of RC members (chord-rotation exceeding (CR) or shear failure (SF)), standard and double IDA analyses were re-evaluated hypothesizing to vary column stirrups spacing. An increase of stirrups interaxis reduces shear strength (V_{Rd}) of columns and consequently shear collapse thresholds defined by Eq. (3).

Previous results have shown that shear failure did not occur for the actual specimen stirrups spacing (S = 150 mm). Anticipated shear collapses were then induced by assuming column stirrup spacing (S) of 250 and 350 mm. D-IDA results in Fig. 19 clearly show the change of the collapse mode with a significant shifting of collapse limit state achievement on the curves with respect to the previously investigated condition (S = 150 mm).

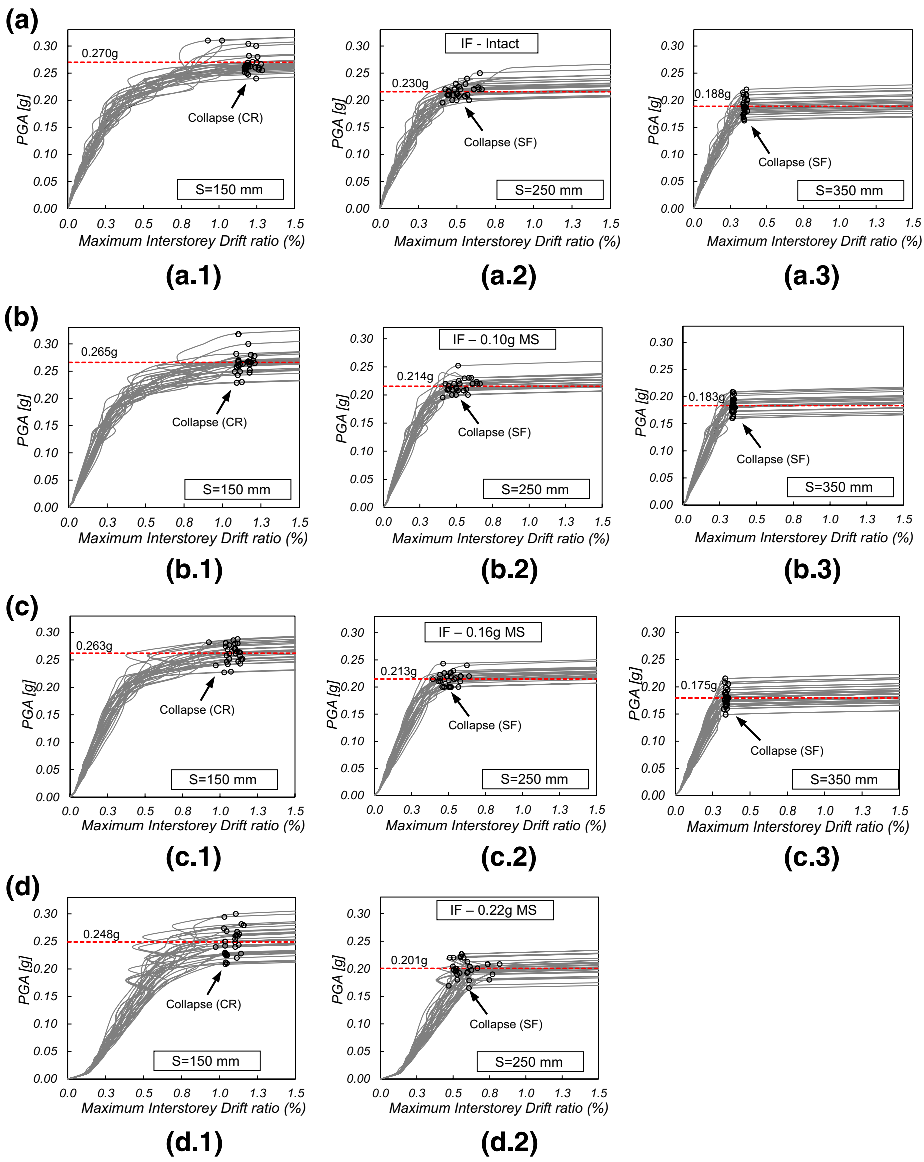

Fig. 19 Standard IDA and aftershock IDA curves of infilled frame and collapse limit state points considering different stirrup spacing (S): **a** intact structure (S = 150, 250 and 350 mm); **b** 0.10 g mainshock (S = 150, 250 and 350 mm); **c** 0.16 g mainshock (S = 150, 250 and 350 mm); **d** 0.22 g mainshock (S = 150 and 250 mm)

The reduction of shear reinforcement in base columns induced anticipated shear collapse where additional shear demand due to infills exceeded local capacity. IDA curves associated with spacing 250 and 350 mm show a dramatic reduction of average collapse PGA and displacement, indicating that shear collapse tends to occur within elastic filed.

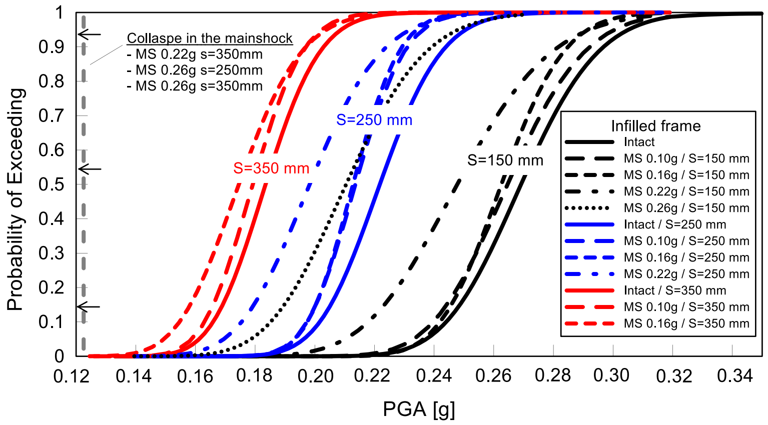

Fig. 20 Intact and aftershock fragility curves of bare and infilled frame with different stirrup spacing (S) of columns

Furthermore the infilled frame collapsed in the mainshock at MS PGA of 0.22 g for 350 mm stirrup spacing and with MS PGA 0.26 g for 250 and 350 mm spacing.

Fragility curves in Fig. 20 show seismic fragility increase of the infilled frame due to shear failure of columns. For the intact case the average collapse PGA (0.27 g) associated with S = 150 mm suffered a reduction of − 19% (0.22 g) with 250 mm spacing and − 30% (0.19 g) with 350 mm spacing. For the aforementioned cases of collapse in the mainshock, aftershock fragility curves are ideally represented with a vertical line at the horizontal axis origin (Fig. 20).

For both 250 and 350 mm spacing cases, residual capacity domains and loss diagrams (Fig. 21) show that aftershock capacity is not substantially reduced with increasing mainshock intensity up to the achievement of the MS PGA values causing collapse

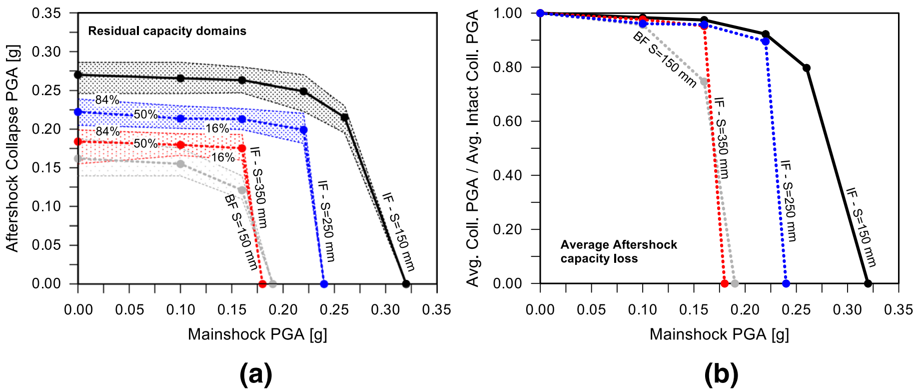

Fig. 21 Residual capacity diagrams of bare and infilled frame considering different stirrup spacing (S): **a** residual capacity domains; **b** aftershock capacity loss diagrams

in the mainshock. Residual capacity suddenly drops to zero when collapse in the mainshock occurs. In Fig. 21a, b, bare frame diagrams are also reported. It can be observed that collapse probability distributions of the infilled frame with S = 350 mm and bare frame overlap at different MS intensities. This means that infilled frame with inadequate shear reinforcement may collapse at lowest MS/AS PGA levels with respect to bare frame.

7 Conclusions

The paper presented a framework to assess seismic fragility and aftershock residual capacity of bare and infilled frames subject to mainshock aftershock sequences. Double incremental dynamic analysis (D-IDA) is proposed as new reference analysis tool, as it combines mainshocks at different intensity levels with a sets of spectrum-compatible aftershocks scaled in amplitude. Results of D-IDA allow defining standard and aftershock fragility curves as well as residual capacity diagrams, representing the reduction of aftershock capacity, in terms of PGA, as a function of mainshock intensity. The reference structural model of a real RC frame prototype structure has been analysed with and without considering the influence of masonry infills. Specific limit state conditions were defined to assess chord rotation exceeding and shear failure due to additional shear demand from infills. From the obtained results, the following conclusions can be drawn:

- Masonry infills provide additional capacity to resist mainshock and aftershock ground motions, limiting damage to primary structures as a consequence of the reduced displacement demand.
- Aftershock capacity of bare and infilled frames depended on mainshock intensity, however, both structures suffered noticeable reduction only when significant mainshock residual drifts occurred. The reduced inelastic demand associated with the infilled frame structure resulted in a reduction of mainshock residual drifts. As consequence of this, infilled frame aftershock fragilities were significantly lower even if compared with that of intact bare frame.
- Residual capacity domains and aftershock loss diagrams confirmed that infilled frame was able to maintain almost all intact capacity even after mainshock intensities causing collapse of bare frame.
- Anticipated shear collapse, due to inadequacy of RC members to support additional shear demand arising from infill-frame interaction, may cause an inversion of the trend. Increasing of stirrups spacing caused severe increase of intact and aftershock fragility. Anticipated shear collapses occurred within quasi-elastic field and even in the mainshock.
- Results allow concluding that, if shear collapse doesn't occur because of local infill-frame interaction, a regular distribution of infills drastically reduces aftershock collapse probability of RC frame structures. The significant structural damage reduction recognized for infilled frames also implies a reduction of costs for repairing primary structures, especially at the lowest ground motion intensities, although repairing costs of masonry infills can result more relevant. Innovative infill solutions, such as infills with sliding panels (e.g. Bolis et al. 2017; Preti and Bolis 2017) may be considered as potential optimal compromise between residual resistance capacity and non-structural damage reduction.

- The study has been carried out on 2D frame because of the large computational demand associated with multiple incremental dynamic analyses. A generalization of results by investigating detailed 3D structures would be desirable.

Acknowledgements This paper was supported by DPC-RELUIS 2014-2018, WP6: Capacità sismica di tamponature ed interventi di rafforzamento.

References

Amadio C, Fragiacomo M, Rajgelj S (2003) The effects of repeated earthquake ground motions on the non-linear response of SDOF systems. Earthq Eng Struct Dyn 32(2):291–308
Asteris PG, Tsaris AK, Cavaleri L, Repapis CC, Papalou A, Di Trapani F, Karypidis DF (2015) Prediction of the fundamental period of infilled RC frame structures using artificial neural networks. Comput Intell Neurosci. https://doi.org/10.1155/2016/5104907
Asteris PG, Cavaleri L, Di Trapani F, Sarhosis V (2016) A macro-modelling approach for the analysis of infilled frame structures considering the effects of openings and vertical loads. Struct Infrastruct Eng 12(5):551–566
Asteris PG, Cavaleri L, Trapani Di, Tsaris AK (2017) Numerical modelling of out-of-plane response of infilled frames: state of the art and future challenges for the equivalent strut macromodels. Eng Struct 132:110–122
Bolis V, Stavridis A, Preti M (2017) Numerical investigation of the in-plane performance of masonry-infilled RC frames with sliding subpanels. J Struct Eng 143(2):04016168
Campione G, Cavaleri L, Macaluso G, Amato G, Di Trapani F (2015) Evaluation of infilled frames: an updated in-plane-stiffness macro-model considering the effects of vertical loads. Bull Earthq Eng 13(8):2265–2281
Campione G, Cavaleri L, Di Trapani F, Macaluso G, Scaduto G (2016) Biaxial deformation and ductility domains for engineered rectangular RC cross-sections: a parametric study highlighting the positive roles of axial load, geometry and materials. Eng Struct 107(15):116–134
Campione G, Cavaleri L, Di Trapani F, Ferrotto MF (2017) Frictional effects in structural behavior of no-end-connected steel-jacketed RC columns: experimental results and new approaches to model numerical and analytical response. J Struct Eng (ASCE) 143(8):04017070
Carvalho EC, Coelho E (2001) Seismic assessment, strengthening and repair of structures. radECOEST2-ICONS report no. 2, European Commission—training and mobility of researchers programme
Cavaleri L, Di Trapani F (2014) Cyclic response of masonry infilled RC frames: experimental results and simplified modeling. Soil Dyn Earthq Eng 65:224–242
Cavaleri L, Di Trapani F (2015) Prediction of the additional shear action on frame members due to infills. Bull Earthq Eng 13(5):1425–1454
Cavaleri L, Di Trapani F, Macaluso G, Papia M (2012) Reliability of code proposed models for assessment of masonry elastic moduli. Ing Sismica 29(1):38–59
Cavaleri L, Di Trapani F, Macaluso G, Papia M, Colajanni P (2014) Definition of diagonal Poisson's ratio and elastic modulus for infill masonry walls. Mater Struct 47(1–2):239–262
Cavaleri L, Di Trapani F, Asteris PG, Sarhosis V (2017) Influence of column shear failure on pushover based assessment of masonry infilled reinforced concrete framed structures: a case study. Soil Dyn Earthq Eng 100:98–112
Celarec D, Dolšek M (2013) Practice-oriented probabilistic seismic performance assessment of infilled frames with consideration of shear failure of columns. Earthq Eng Struct Dyn 42:1339–1360
D.M. LL. PP. 14.01.2008 (2008) Nuove norme tecniche per le costruzioni
Di Sarno L (2013) Effects of multiple earthquakes on inelastic structural response. Eng Struct 56:673–681
Di Trapani F, Macaluso G, Cavaleri L, Papia M (2015) Masonry infills and RC frames interaction: literature overview and state of the art of macromodeling approach. Eur J Environ Civil Eng 19(9):1059–1095
Di Trapani F, Bertagnoli G, Ferrotto MF, Gino D (2018a) Empirical equations for the direct definition of stress-strain laws for fiber-section based macro-modeling of infilled frames. J Eng Mech (ASCE). https://doi.org/10.1061/(ASCE)EM.1943-7889.0001532
Di Trapani F, Shing PB, Cavaleri L (2018b) Macroelement model for in-plane and out-of-plane responses of masonry infills in frame structures. J Struct Eng (ASCE) 144(2):04017198

Dolšek M, Fajfar P (2008) The effect of masonry infills on the seismic response of four storey reinforced concrete frame—a deterministic assessment. Eng Struct 30(7):1991–2001

El-Dakhakhni W, Elgaaly M, Hamid A (2003) Three-Strut model for concrete masonryinfilled steel frames. J Struct Eng (ASCE) 129(2):177–185

Eurocode 8 (2004) Design of structures for earthquake resistance—Part 1: general rules, seismic actions and rules for buildings. European Committee for Standardization, Brussels

Fragiacomo M, Amadio C, Macorini L (2004) Seismic response of steel frames under repeated earthquake ground motions. Eng Struct 26(13):2021–2035

Hatzigeorgiou GD, Liolios AA (2010) Nonlinear behaviour of RC frames under repeated strong ground motions. Soil Dyn Earthq Eng 30:1010–1025

Hatzivassiliou M, Hatzigeorgiou GD (2015) Seismic sequence effects on three-dimensional reinforced concrete buildings. Soil Dyn Earthq Eng 72:77–88

Hosseinpour F, Abdelnaby AE (2017a) Effect of different aspects of multiple earthquakes on the nonlinear behavior of RC structures. Soil Dyn Earthq Eng 92:706–725

Hosseinpour F, Abdelnaby AE (2017b) Fragility curves for RC frames under multiple earthquakes. Soil Dyn Earthq Eng 98:222–234

Jeon JS, Park JH, DesRoches R (2015) Seismic fragility of lightly reinforced concrete frames with masonry infills. Earthq Eng Struct Dyn 44:1783–1803

Li Y, Song R, Van De Lindt JW (2014) Application of reliability-based robustness assessment of steel moment resisting frame structures under post-mainshock cascading events. J Struct Eng (ASCE) 140(12):04014095

Mainstone RJ (1974) Supplementary note on the stiffness and strength of infilled frames. Building research station, current paper CP 13/74, UK

McKenna F, Fenves GL, Scott MH (2000) Open system for earthquake engineering simulation. University of California, Berkeley

Pantò B, Caliò I, Lourenço PB (2017) Seismic safety evaluation of reinforced concrete masonry infilled frames using macro modelling approach. Bull Earthq Eng 15(9):3871–3895

Preti M, Bolis V (2017) Masonry infill construction and retrofit technique for the infill-frame interaction mitigation: test results. Eng Struct 132:597–608

Raghunandan M, Liel AB, Luco N (2015) Aftershock collapse vulnerability assessment of reinforced concrete frame structures. Earthq Eng Struct Dyn 44(3):419–439

Ribeiro FLA, Barbosa AR, Neves LC (2014) Application of reliability-based robustness assessment of steel moment resisting frame structures under post-mainshock cascading events. J Struct Eng (ASCE) 140(8):A4014008

Vamvatsikos D, Cornell AC (2002) Incremental dynamic analysis. Earthq Eng Struct Dyn 31(3):491–514

Varum H (2003) Seismic assessment, strengthening and repair of existing buildings. University of Aveiro, Portugal

Vanmarcke EH, Cornell CA, Gasparini DA, Hou S (1976) SIMQKE-I: Simulation of earthquake ground motions. https://nisee.berkeley.edu/elibrary/getpkg?id=SIMQKE1. Accessed 31 July 2017